ACS APPLIED MATERIALS & INTERFACES

Research Article

www.acsami.org

Bioreducible Cross-Linked Hyaluronic Acid/Calcium Phosphate Hybrid Nanoparticles for Specific Delivery of siRNA in Melanoma Tumor Therapy

Zhanwei Zhou,[†] Huipeng Li,[†] Kaikai Wang,[†,‡] Qian Guo,[†] Chenzi Li,[†] Hulin Jiang,[†] Yiqiao Hu,[‡] David Oupicky,[†,§] and Minjie Sun*[,†]

[†]State Key Laboratory of Natural Medicines and Department of Pharmaceutics, China Pharmaceutical University, Nanjing 210009, China

[‡]State Key Laboratory of Pharmaceutical Biotechnology, Medical School, Nanjing University, Nanjing 210093, China

[§]Department of Pharmaceutical Sciences, Center for Drug Delivery and Nanomedicine, University of Nebraska Medical Center, Omaha, Nebraska 68198, United States

Supporting Information

ABSTRACT: This study introduces a novel cross-linking strategy capable of successfully stabilizing CaP nanoparticles and stimuli-responsive small interfering RNA (siRNA) release. We synthesized a polysaccharide derivative thiolated hyaluronic acid (HA-SH), which was slightly modified but multifunctional and developed a smart redox-responsive delivery system. siRNA was efficaciously condensed by calcium phosphate (CaP) via electrostatic interaction to form a positively charged inner "core". Disulfide cross-linked HA (HA-ss-HA) was formed and played a role as an anionic outer "shell" to stabilize the CaP core. We demonstrated that the nanoparticles were stable both in the storage milieu and systemic circulation, thus overcoming the most serious disadvantage of CaP nanoparticles for gene delivery. Meanwhile, this smart system could selectively release siRNA into the cytosol by both a GSH-triggered disassembly and successful endosomal escape. Therefore, the hybrid delivery system achieved an 80% gene-silencing efficiency in vitro for both luciferase and Bcl2. Silencing of Bcl2 resulted in dramatic apoptosis of B16F10 cells. Besides, equipped with the tumor-targeting component HA, the nanoparticles significantly suppressed the growth of B16F10 xenograft tumor in mice. The anionic HA-ss-HA-equipped nanoparticles showed no apparent toxicity in vitro or in vivo, as well as showed a high transfection efficiency. Taken together, this redox-responsive, tumor-targeting smart anionic nanoparticle holds great promise for exploitation in functionalized siRNA delivery and tumor therapy.

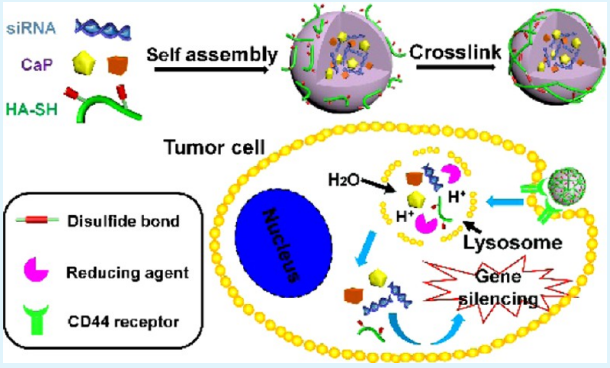

KEYWORDS: *redox responsive, calcium phosphate, hyaluronic acid, hybrid nanoparticles, siRNA delivery, antitumor*

INTRODUCTION

Small interfering RNA (siRNA) holds tremendous promise for tumor therapy.[1] Viral and nonviral carriers have been widely used for siRNA delivery.[2] Although the viral carriers show a high transfection efficiency, serious immunotoxicity and side effects enormously limit their applications.[3] Cationic lipids, polymers, and inorganic materials, the most popular nonviral carriers, can condense siRNA efficiently by forming nanoparticles, which significantly improves the cell uptake and gene-silencing efficiency.[4−6]

Among all of the nonviral vectors that have been investigated, calcium phosphate (CaP) shows prominent advantages of high transfection efficiency and biocompatibility.[7,8] However, its rapid and uncontrollable crystal growth and lack of tissue specificity greatly limits its clinical application.[9,10] Many strategies have been employed to solve these problems, such as combining CaP with dopa-HA[11] or anionic lipid DOPA.[12] Dr. Kataoka's group[13] reported a bioreducible CaP nanosystem for siRNA delivery. Thiolated poly(ethylene glycol) (PEG) was conjugated with siRNA-SH by a disulfide bond, forming PEG-SS-siRNA. An intracellular redox environment could trigger siRNA release from the nanocomposites. In our previous study,[14] PEG-CMCS was used as an anionic polymer to stabilize CaP particles and to deliver siRNA effectively. Nevertheless, most hybrid systems have focused on improving the stability of CaP particles. Hybrid systems that incorporate tumor-targeting or stimuli-responsive properties, or both, have rarely been described in recent research.

Received: November 30, 2016
Accepted: April 10, 2017
Published: April 10, 2017

DOI: 10.1021/acsami.6b15347
ACS Appl. Mater. Interfaces 2017, 9, 14576−14589

Scheme 1. (A) Schematic Illustration of a Cross-Linked Anionic Delivery System, Consisting of siRNA-Loaded HA-SH/CaP Hybrid Nanoparticles ($NP_{HA\text{-}SH/CaP}$/siRNA); (B) Schematic Illustration of Tumor-Targeted siRNA Delivery by HA-SH/CaP Nanoparticles[a]

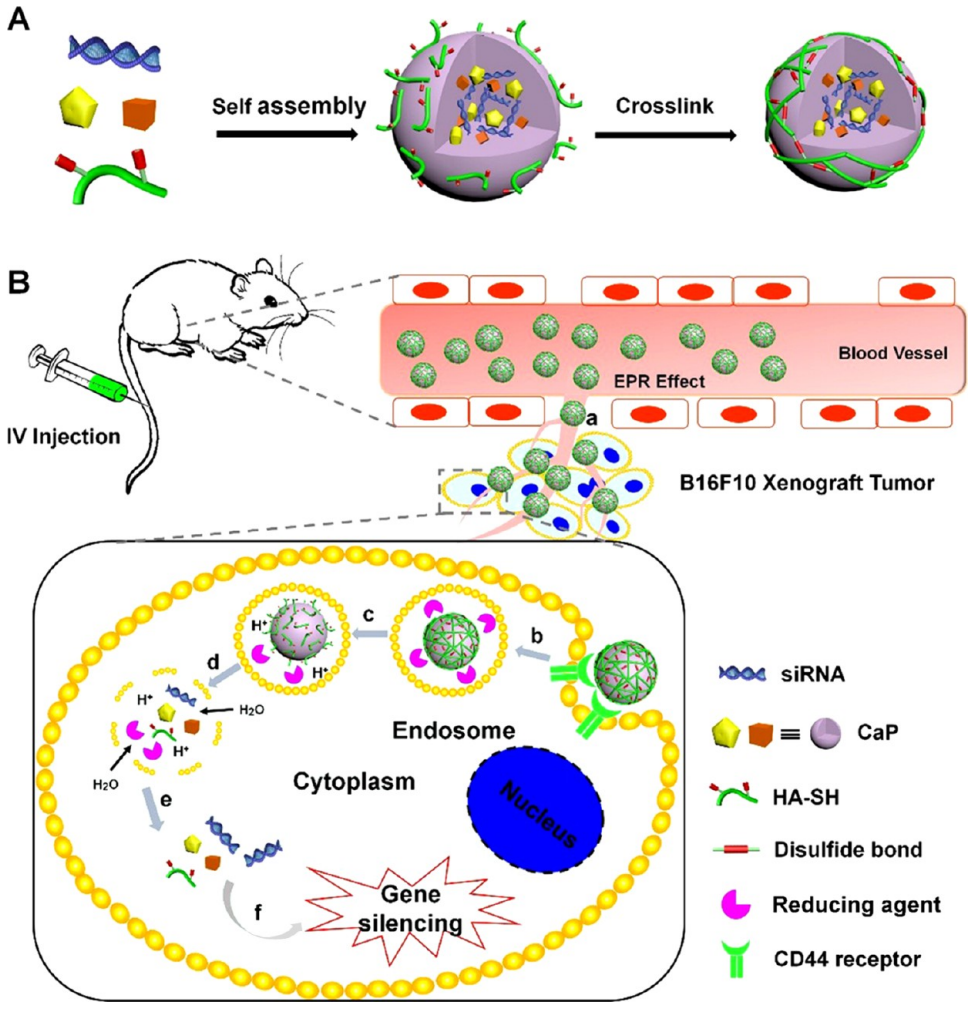

[a](A) The HA-SH shell of freshly prepared nanoparticles is loose because it is held together only by the electrostatic interaction between HA-SH and the CaP core. However, after exposure to air for some time, the structure becomes tight because of cross-linking of the thiol groups and formation of the disulfide bonds. (B) (a) Accumulation of $NP_{HA\text{-}SH/CaP}$/siRNA at tumor sites through passive and active targeting, (b) receptor-mediated uptake of NPs by B16F10 cells, (c) redox-triggered destruction of the HA-ss-HA shell and exposure of the CaP core to the acidic endosome or lysosome, (d) dissolution of CaP and increase in osmotic pressure, (e) endosomal escape, and (f) target gene silencing.

Carriers responding to various stimuli (e.g., light,[15] heat,[16] redox,[17] and pH[14]) have been widely developed to promote physiological specificity and on-demand therapeutic efficacy delivery of anticancer drugs or nucleic acids.[18] Among these stimuli, redox shows great potential owing to the redox environment in the intracellular space. The concentration of the reducing agent, glutathione, in cytosol (approximately 2−10 mM) is much higher than that in the mildly oxidizing extracellular spacer, which is approximately 2−20 μM. In addition, endosomes and lysosomes are also redox-active and are modulated by reducing enzyme γ-interferon-inducible lysosomal thiol reductase in combination with cysteine.[19−21] Redox-responsive delivery systems with cross-linked disulfide bonds can maintain adequate stability in the circulation and extracellular milieu before undergoing rapid cleavage when exposed to the reducing conditions within the cell. By taking advantage of this feature, many redox-responsive nanocarriers for nucleic acids or chemical drugs have been prepared to achieve a burst of drug release in tumor cells.[22,23]

Hyaluronic acid (HA), a natural anionic polysaccharide, has been commonly applied in plastic surgery and arthritis treatment in the clinic because of its high biocompatibility and low immunogenicity.[24] Furthermore, as reported, receptors of HA, such as CD44, are overexpressed in various cancer cells.[25] Recently, because of this CD44 targeting characteristic, HA and its derivatives have been widely used as target-specific delivery vehicles for various therapeutic agents.[24−26]

Herein, a hybrid nanoparticle based on CaP and cross-linked HA-ss-HA, with dual functions of redox responsiveness and specific tumor targeting, was explored as an siRNA carrier for melanoma therapy (Scheme 1A). siRNA was efficaciously condensed by CaP via electrostatic interactions, forming a positively charged inner core. HA-ss-HA acted as an anionic outer shell to stabilize and compress the particles. The hybrid nanoparticles could selectively release siRNA into the cytosol due to the intracellular reducible environment, and the siRNA could successfully escape from the endosomes because of the membranolytic property of CaP (Scheme 1B). A slight

DOI: 10.1021/acsami.6b15347
ACS Appl. Mater. Interfaces 2017, 9, 14576−14589

modification of thiolated-HA (HA-SH) was carried out to facilitate the formation of cross-linked HA-ss-HA in the hybrid CaP nanoparticles by oxidation in air. The gene encoding Bcl2, an antiapoptosis protein, was utilized as our therapeutic target gene. B16F10 cells (mouse melanoma tumor cells), which overexpress the CD44 receptor, and tumor xenograft models derived from B16F10 were used to evaluate in vitro gene transfection efficiency and in vivo antitumor efficacy. In addition, the safety of this system was evaluated both in vitro and in vivo.

EXPERIMENTAL SECTION

Materials, Cell Culture, and Animals. Sodium HA (molecular weight 450 kDa) was purchased from Zhenjiang Dongyuan Biotechnology Co., Ltd. (Jiangsu, China). 1-Ethyl-3-(3-dimethylaminopropyl) carbodiimide hydrochloride (EDC·HCl), hydroxybenzotriazole (HOBT), DL-dithiothreitol (DTT), and cystamine dihydrochloride (cys) were purchased from Shanghai Dibo Reagent Co. Ltd. (Shanghai, China). The BCA Kit was purchased from Thermo (Rockford, IL). Trypsin EDTA solution, penicillin streptomycin solution, RPMI-1640 medium, the Annexin V-FITC/PI Apoptosis Detection Kit, and MTT were purchased from KeyGen biotech (Nanjing, China). Fetal bovine serum (FBS) was purchased from Gibco (Thermo Fisher Scientific).

siNC (negative control), FAM-siNC, cy3-siNC, siLuc (targeting luciferase), and siBcl2 (targeting Bcl2) were synthesized by Genepharma (Shanghai, China). Cy5-siNC was synthesized by RiboBio (Guangzhou, China). Bcl2-specific antibody (50E3) rabbit mAb,[27] β-tubulin (9F3) rabbit mAb, and HRP-linked antirabbit IgG were purchased from Cell Signaling Technology. The siRNA sequences were depicted as below

siNC, sense strand, 5′-UUC UCC GAA CGU GUC ACG UTT-3′

siLuc, sense strand, 5′-GGA CGA GGA CGA GCA CUU CUU-3′

siBcl2, sense strand, 5′-GCA UGC GAC CUC UGU UUG AdTdT-3′

B16F10 mouse melanoma cells were obtained from American Type Culture Collection and cultured in RMPI 1640 medium; they were supplemented with 10% FBS and 1% penicillin/streptomycin at 37 °C in a humidified 5% CO_2 incubator. Cells were cultured in a 25 cm^2 tissue culture flask and passaged every other day.

Male C57BL/6 mice (18−22 g) and male BALB/c mice (18−22 g) were bought from Shanghai Jiesijie Laboratory Animal Limited Company. All of the animal experiments were performed in compliance with the Guide for Care and Use of Laboratory Animals, approved by China Pharmaceutical University.

Synthesis and Characterization of HA-SH. The synthesis of thiolated-HA was carried out on the basis of a previously reported procedure.[28] Briefly, HA (200 mg, MW 450 kDa, 0.5 mmol) was dissolved in PBS solution (pH 6.8). Eight molar excess of EDC (766.8 mg, 4 mmol) and *N*-HOBT (540.6 mg, 4 mmol) were reacted with HA for 2 h, and then cystamine (617.2 mg, 4 mmol) was added and stirred for 24 h. Later, a dialysis treatment was done for 48 h. Subsequently, the pH was adjusted to 8.5 and the solution was treated with DTT for 2 h. The product was dialyzed against deionized water (pH was adjusted to 3 with HCl) for 48 h (MW cutoff 8−12 kDa). The degree of substitution (DS), which is defined as the number of free thiol groups per 100 monomers, was analyzed by Ellman's assay,[29] ^{1}H NMR spectroscopy (using D_2O), and Fourier-transform infrared (FTIR) measurement. The final product was freeze-dried and stored at −20 °C.

Preparation of $NP_{HA\text{-}SH/CaP}$/siRNA. $CaCl_2$ solution (30 μL, 2.5 M) was first added to siRNA (30 μL, 60 μM) solution. Later, 240 μL of Tris buffer (1 mM Tris·HCl, pH 7.4) was added to the final volume of 300 μL. After incubation for 1 min, 300 μL of this Ca^{2+}/siRNA solution was quickly added to an equal volume of HEPES/phosphate/HA-SH solution (140 mM NaCl, 50 mM HEPES, 1.5 mM Na_2HPO_4, 1 mg/mL HA-SH, pH 7.4) with a vortex. Subsequently, the excess free calcium ions were removed by ultrafiltration. This prepared solution (600 μL) was transferred to an ultrafiltration tube (MW cutoff 10 kDa) containing 600 μL of an extracellular buffer (2 mM $CaCl_2$, 1 mM Na_2HPO_4, 25 mM Tris, 140 mM NaCl, pH 7.4). The nanoparticle-containing solution was centrifuged at 4000*g* for 30 min. After centrifugation, the solution retained in the inner tube was collected and used for further experiments.

Degree of Cross-Linking of HA-SS-HA. The degree of cross-linking of HA-SS-HA was defined by the formula below, and the concentration of free thiol in the preparation was investigated by Ellman's assay.

$$\text{degree of cross-linking}\ (\%) = (C_0 - C_t)/C_0$$

where C_0 is the concentration of free thiol in freshly prepared formulations and C_t is the concentration of free thiol in the formulations after incubation for some time (t).

Particle Size, Size Distribution, ζ Potential, and Morphological Observation. The particle size, polydispersity index, and ζ potential of $NP_{HA\text{-}SH/CaP}$/siRNA were determined using Brookhaven Instruments-Zeta Plus (Brookhaven, NY) at 0 and 12 h after preparation. An H-600 transmission electron microscope (TEM) (Hitachi, Japan) was used to visualize the morphology of the nanoparticles 12 h after preparation.

Encapsulation Efficiency (EE) of $NP_{HA\text{-}SH/CaP}$/siRNA. Free siRNA were detected using a Ribogreen assay. To precipitate the nanoparticles, 200 μL of the nanoparticle solution was centrifuged at 15 000*g* for 30 min. Later, 100 μL of supernatants were collected and mixed with 100 μL Ribogreen solution (Molecular Probes, Eugene). After 5 min, the fluorescence of the mixture was detected by a GloMax-Multi Jr Single Tube Multimode Reader (Promega). EE is calculated as below

$$\text{encapsulation efficiency}\ (\%) = (C_{total} - C_{unloaded})/C_{total} \times 100\%$$

where C_{total} is the concentration of the total siRNA in the mixture and $C_{unloaded}$ represents the concentration of free siRNA unloaded by the nanoparticles.

Colloidal Stability, RNase Stability, and Serum Stability. To know the colloidal stability, different formulations (CaP/siRNA, HA/CaP/siRNA, HA-SS-HA/CaP/siRNA) were incubated at 4 °C and the particle size was monitored at different time intervals by dynamic light scattering (DLS).

Poor stability in the serum and enzymatic degradation are the main factors hindering effective siRNA delivery in vivo. To evaluate the superior protective effect of $NP_{HA\text{-}SH/CaP}$ on siRNA, naked siRNA and different formulations of siRNA (CaP/siRNA, HA/CaP/siRNA, HA-SS-HA/CaP/siRNA) (20 μL, siRNA concentration was 20 μg/mL) were incubated with RNase I (2 μL, 5 U/μL) or rat serum (v/v = 1:1) for different times (0, 2, 4, 8, 16, 24, and 48 h). Sodium dodecyl sulfate (SDS) (2%) was then added to dissociate the nanoparticles and release the siRNA. Agarose gel electrophoresis was used to detect the siRNA intensity of each sample.

Disassembly of $NP_{HA\text{-}SH/CaP}$/siRNA Triggered by GSH and in Vitro Release of siRNA. Disassembly of $NP_{HA\text{-}SH/CaP}$/siRNA in response to 10 mM GSH was monitored by DLS to observe the change in particle size. The disruption of nanoparticles was further observed by TEM imaging. For in vitro release studies, siRNA-loaded nanoparticles were incubated at four different conditions: pH 7.4 with or without 10 μM GSH and pH 5.0 with or without 10 mM GSH. Each sample was collected at 0 and 2 h and analyzed by gel electrophoresis in Tris-borate buffer on a 2% agarose gel.

Cell Uptake and Intracellular Distribution of $NP_{HA\text{-}SH/CaP}$/siRNA. *Flow Cytometry Analysis.* For flow cytometric analyzes, B16F10 cells (5×10^4) were seeded into 24-well plates. When the cells reached 80% confluence, the culture medium was replaced with $NP_{HA\text{-}SH/CaP}$/FAM-siRNA and free FAM-siRNA containing medium. The dose of FAM-siRNA was 100 nM. Untreated cells were used as a negative control. After the cells were cultured in the incubator for different times (1, 2, and 4 h), cellular uptake was stopped with cold PBS. The cells were then collected by trypsinization, and the fluorescence intensity was measured using a flow cytometer.

DOI: 10.1021/acsami.6b15347
ACS Appl. Mater. Interfaces 2017, 9, 14576−14589

To further investigate the cellular uptake mechanism, cells were preincubated with different inhibitors for 30 min at 37 °C, including chlorpromazine, amiloride, NaN_3, and nystatin (the concentrations were 10, 1.3, 1, and 20 mg/mL, respectively). After pretreatment, the cells were incubated with FAM-siRNA-loaded nanoparticles for 2 h.

In addition, to determine the effect of CD44 receptors on cellular uptake, cells were pretreated with different concentrations of free HA (2.5, 5, 10 mg/mL) for 30 min to block the CD44 receptors, which promote the uptake of HA-conjugated nanoparticles via receptor-mediated endocytosis.[30] After pretreatment, the cells were also incubated with $NP_{HA\text{-}SH/CaP}$/FAM-siRNA for 2 h.

Confocal Laser Scanning Microscopy (CLSM) Observation. B16F10 cells were seeded in 20 mm confocal microscopy dishes at a concentration of 5×10^4 cells/well. When the cells reached 60% confluence, they were treated with $NP_{HA\text{-}SH/CaP}$/FAM-siRNA (siRNA = 100 nM) for 2 h at 37 °C and then washed twice with PBS and fixed with 4% paraformaldehyde for 10 min. DAPI was then added to stain the cell nuclei. The cellular uptake of nanoparticles was visualized using a Zeiss CLSM. The images were analyzed using Zeiss CLSM software.

For further observation of endosomal escape, endosomes and lysosomes of B16F10 cells were stained with LysoTracker Red for 15 min in the dark after different incubation times (1, 3, and 5 h), with $NP_{HA\text{-}SH/CaP}$/FAM-siRNA. The cells were then washed with PBS three times prior to CLSM imaging.

The redox-triggered release of siRNA in the cells was studied via fluorescence resonance energy transfer (FRET). Cy3 and cy5 were used as a FRET pair and co-loaded into the nanoparticles.[31,32] Cy3-siRNA and cy5-siRNA were used at a ratio of 1:1 and the total siRNA dosage was 100 nM. FRET nanoparticles were confirmed by fluorescence spectra. The FRET nanoparticles were treated with 10 mM GSH for different times (0, 1, 2, and 4 h), and then the fluorescence spectra were detected with a 512 nm excitation luminescence. In cell study, *N*-ethyl maleimide (NEM) was used to deplete the intracellular GSH. B16F10 cells were incubated with the FRET-NPs for 2 h. A longer incubation time of 5 h with or without 1 mM NEM pretreatment for 30 min was also studied, and then CLSM images were captured. The observation parameters of CLSM is Cy3 $\lambda_{exc/em}$ 550/570 nm, Cy5 $\lambda_{exc/em}$ 550/670 nm.

In Vitro Gene Silencing. *siRNA Silencing of Luciferase.* B16F10-luciferase cells were seeded in 24-well plates at a density of 5×10^4 cells per well 24 h prior to the experiments. Cells were transfected with nanoparticles loaded with siLuc at different dosage (25, 50, 100, 200 nM). Cells were also treated with $NP_{HA\text{-}SH/CaP}$/siNC containing 200 nM siNC, 200 nM free siLuc and PBS as negative controls. Polyethyleneimine (PEI, 25 kDa) loaded with 100 nM siLuc was used as a positive control. After incubation for 4 h, the transfection solution was replaced with medium containing 10% FBS and the cells were incubated for another 24 h. The cells were then washed with cold PBS twice and lysed with RIPA lysis buffer. The luciferase activity was measured by a microplate reader (BioTek Synergy2) using a luciferase assay kit (Beyotime, China). The siRNA-mediated luciferase silencing efficiencies were normalized to the total cell protein concentration and expressed as percent luciferase activity of untreated cells.

siRNA Silencing of Bcl2. B16F10 cells were dispensed into 12-well plates (1×10^5 cells/well) and incubated to reach 70% confluence. Various formulations, including $NP_{HA\text{-}SH/CaP}$/siBcl2 (50, 100 nM), PEI/siBcl2 (100 nM), free siBcl2 (100 nM), $NP_{HA\text{-}SH/CaP}$/siNC (100 nM), and PBS, were added to the cells and incubated for 4 h. Cells were then incubated with fresh 1640 medium for 44 h.

For analysis of Bcl2 protein expression, the $NP_{HA\text{-}SH/CaP}$/siBcl2-treated cells were washed twice with cold PBS, and then 100 μL per well of RIPA lysis buffer (Beyotime) supplemented with 1% of phenylmethylsulfonyl fluoride was added. After incubation for 30 min on ice, the cell lysates were centrifuged at 4 °C at 12 000 rpm for 20 min. The protein concentration was determined using the BCA kit. Each formulation was separated on a 12% SDS-PAGE gel and then transferred onto a 0.45 μm poly(vinylidene difluoride) membrane (Millipore). After blocking in 5% of nonfat milk in PBS-Tween-20 (PBS-T, pH 7.4) at room temperature for 1 h, the membrane was incubated in 5% of milk in PBS-T with Bcl2-specific rabbit monoclonal antibody (1:1000) and β-tubulin rabbit monoclonal antibody (1:1000) overnight at 4 °C. After incubation in 5% of milk with goat antirabbit IgG/HRP (1:5000) (Abcam) for 1 h, protein bands were visualized using Tanon High-sig ECL substrate (Tanon, China).

Cell Apoptosis Assay. Apoptosis of B16F10 cells was detected using the Annexin V-FITC Apoptosis Detection Kit. The cells (1×10^5 cells per well) were seeded in 12-well plates. After culture for 24 h, the cells were transfected with the same method, as shown in Bcl2 silencing experiment. The subsequent procedures were performed in accordance with the manufacturers protocol. Annexin V-FITC stained the phosphatidylserine that translocate to the extracellular membrane upon early apoptosis, whereas PI stained the intracellular DNA in late apoptotic cells. For Annexin V-FITC apoptosis detection, the cells were analyzed by flow cytometry (BD FACSCalibur).

In Vivo Luciferase Gene-Silencing Study. For the establishment of tumor xenograft models, male C57BL/6 mice (18−22 g) were subcutaneously inoculated with 1×10^5 B16F10-luciferase cells and the tumors were allowed to grow until they were about 600 mm^3. Randomly, the mice were divided into two groups ($n = 3$) and injected with $NP_{HA\text{-}SH/CaP}$/siNC and $NP_{HA\text{-}SH/CaP}$/siLuc (siRNA 1.2 mg/kg) via the tail vein on days 0 and 1. The mice were imaged on days 0 and 2 with a Kodak multimodal-imaging system IS2000MM (Kodak). Before imaging, each mouse was injected with 200 μL of D-luciferin (Dibo, Shanghai) dissolved in saline at a concentration of 15 mg/mL via intraperitoneal injection. At day 2, after being photographed, the mice were then euthanized and the tumor was removed. The tumors were lysed in RIPA lysis buffer, and the lysates were centrifuged at 12 000*g* for 15 min. The supernatant was collected, and the luciferase activity was measured using the same method as in vitro study.

Tumor Suppression Study. *Antitumor Efficacy of $NP_{HA\text{-}SH/CaP}$/siRNA in Vivo.* To confirm the anticancer effect in vivo, the B16F10 tumor xenograft model was established as described above, and anticancer treatments were performed when tumors were around 80 mm^3. The mice were randomly divided into three groups ($n = 5$) and each mouse was injected every other day with PBS, $NP_{HA\text{-}SH/CaP}$/siNC and $NP_{HA\text{-}SH/CaP}$/siBcl2 at a dose of 1.2 mg/kg on days 0, 2, 4, 6, and 8. The tumor size and body weight of the mice were recorded every day for 10 days. The tumor volume was calculated according to the following formula: tumor volume (mm^3) = 0.5 × length × width^2. After 10 days of observation, pictures were taken of representative mice in each of the three groups. Mice were sacrificed on day 10, and the tumor of each mouse was collected and weighed.

Analysis of Bcl2 Protein Expression. To further evaluate the expression level of Bcl2 protein in vivo after five injections, tumors were removed from each mouse and Bcl2 expression was assessed in tumor sections using the same method as in vitro experiment.

H&E Staining and TUNEL Analysis. Tumors were fixed for 24 h in 4% paraformaldehyde, and then paraffin sections were prepared. Hematoxylin/eosin (H&E) staining was carried out for histological analysis, and the TdT-mediated dUTP Nick-End Labeling (TUNEL) assay was used to assess the levels of cell apoptosis in the tumor.

Safety Studies. *Cytotoxicity Evaluation.* The cytotoxicity of HA-SH and $NP_{HA\text{-}SH/CaP}$/siRNA was evaluated using the MTT assay. B16F10 cells were seeded at a density of 5×10^3 cells/well in a 96-well plate and incubated for 24 h. The cells were then incubated with HA-SH (at equivalent HA-SH concentrations of 50, 100, 200, 400, 800, 1000 μg/mL) and $NP_{HA\text{-}SH/CaP}$/siNC (siNC concentrations of 10, 25, 50, 100, 200, 400, 600, 800, 1000 nM) for 24 and 48 h, respectively. After incubation, MTT solution (20 μL, 5 mg/mL in PBS) was added to each well and the cells were incubated for 4 h at 37 °C. The medium was then carefully removed, and then 150 μL of DMSO was added to each well. Absorbance was quantified at 490 nm using a microplate reader. Cell viability was calculated as percentage of the control using the formula (OD of the test group/OD of the control group) × 100 ($n = 4$).

Whole Blood Analysis, Serum Biochemistry, and Histological Evaluation. For the safety evaluation, 10 male BALB/c mice were randomly divided into two groups ($n = 5$) and PBS or $NP_{HA\text{-}SH/CaP}$/siBcl2 (siBcl2 1.2 mg/kg) were injected into mice via intravenous (iv)

DOI: 10.1021/acsami.6b15347
ACS Appl. Mater. Interfaces 2017, 9, 14576−14589

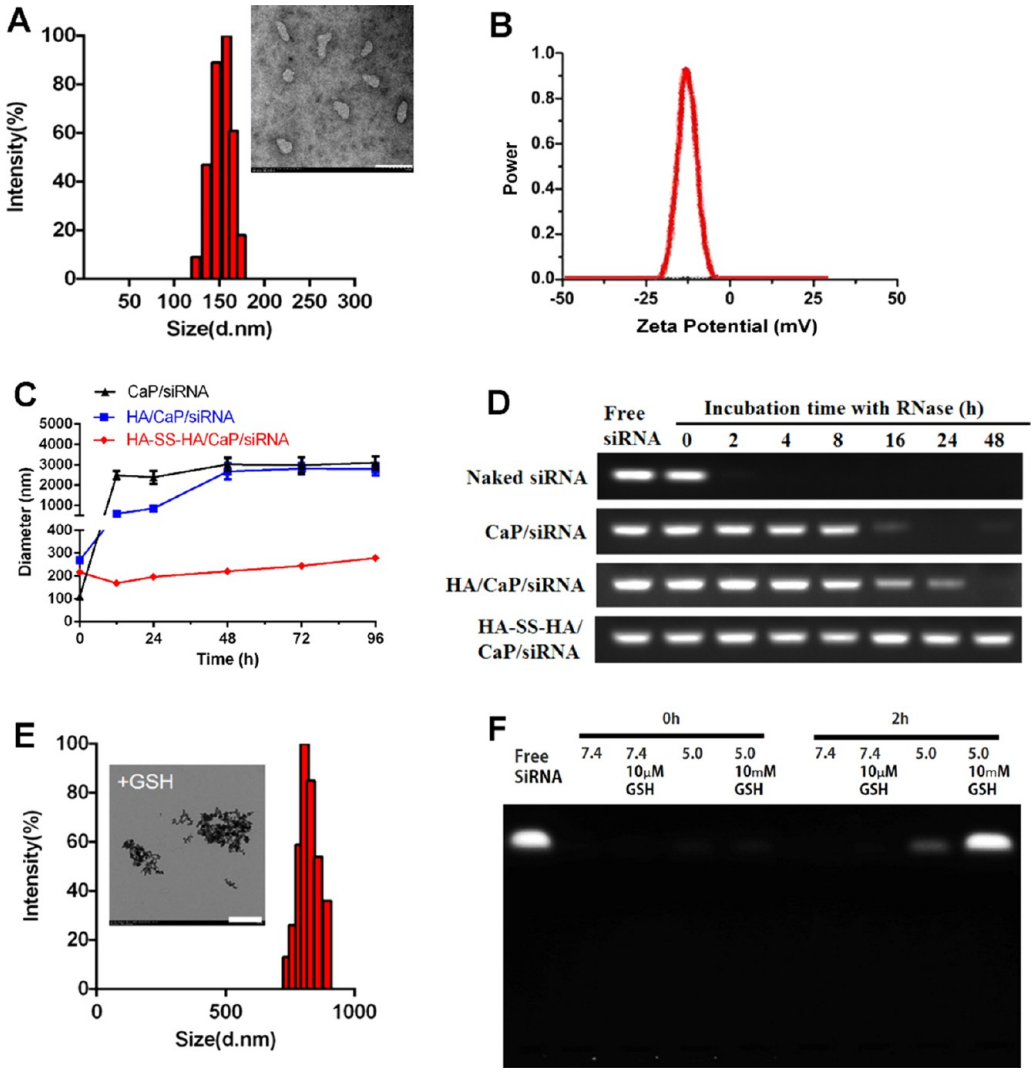

Figure 1. (A) Size distribution of $NP_{HA\text{-}SH/CaP}$/siRNA by DLS and TEM. TEM scale bar: 200 nm. (B) ζ-Potential of $NP_{HA\text{-}SH/CaP}$/siRNA. (C) Variation in the size of CaP/siRNA, HA/CaP/siRNA and HA-SS-HA/CaP/siRNA nanoparticles at storage condition (n = 3). (D) RNase stability of naked siRNA, CaP/siRNA, HA/CaP/siRNA, and HA-SS-HA/CaP/siRNA, determined by agarose gel electrophoresis. (E) Size distribution histogram of $NP_{HA\text{-}SH/CaP}$/siRNA after incubation with 10 mM GSH for 2 h by DLS. Inset: Morphological observation of the treated $NP_{HA\text{-}SH/CaP}$/siRNA by TEM. Scale bar: 500 nm. (F) Release of siRNA at different conditions: pH 7.4 with or without 10 μM GSH and pH 5.0 with or without 10 mM GSH at 0 and 2 h.

on days 0, 2, and 4. Blood was collected on day 5 to check the liver toxicity by testing the levels of alanine transaminase (ALT) and aspartate transaminase (AST) and kidney toxicity by testing the levels of blood urea nitrogen (BUN). The animals were then sacrificed and the major organs (heart, liver, spleen, lung, and kidney) were collected for H&E staining.

Statistical Analysis. All quantitative data are expressed as mean ± S.D. unless otherwise noted. Single factorial analysis of variance (ANOVA) was performed to determine the statistical significance of the data.

RESULTS AND DISCUSSION

Synthesis and Characterization of HA-SH. In this study, the carboxyl groups in HA were functionalized to thiol groups by a simple two-step reaction, as shown in Figure S1A. Firstly, the carboxyl groups of HA were activated by EDC and HOBT. Cystamine was then connected to HA by amidation reaction. Secondly, DTT was used to break up the disulfide bonds to obtain HA-SH.

The chemical structure of HA-SH was confirmed by ^{1}H NMR. As shown in Figure S1B, the structure of HA-SH was confirmed by the characteristic peaks at 2.0 ppm ($\mathbf{CH_3}$—CO—NH_2), 2.7 ppm (NH—$\mathbf{CH_2}$—CH_2—SH). There was a sharp increase at 3.7 nm among 3.3–4.0 nm peaks group, which was speculated to be ascribed to NH—CH_2—$\mathbf{CH_2}$—SH. We then calculated the DS from the peak areas and found that the DS of free thiol is 40.1%. This result was consistent with the quantification of thiol groups by Ellman's assay. Besides, FTIR spectra (Figure S1C) showed a weak peak of thiol (ν, 2529 cm^{-1}), which indicated the successful conjugation of thiol to HA.

Degree of Cross-Linking of HA-SS-HA. The degree of cross-linking of HA-SS-HA was investigated by Ellman's assay and it increased with the longer incubation time (Figure S2).

Preparation and Characterization of $NP_{HA\text{-}SH/CaP}$/siRNA. Stabilized $NP_{HA\text{-}SH/CaP}$/siRNA nanoparticles were prepared by the nanoprecipitation method as described in our previous work.[14] Calcium and phosphate ionic solutions

DOI: 10.1021/acsami.6b15347
ACS Appl. Mater. Interfaces 2017, 9, 14576–14589

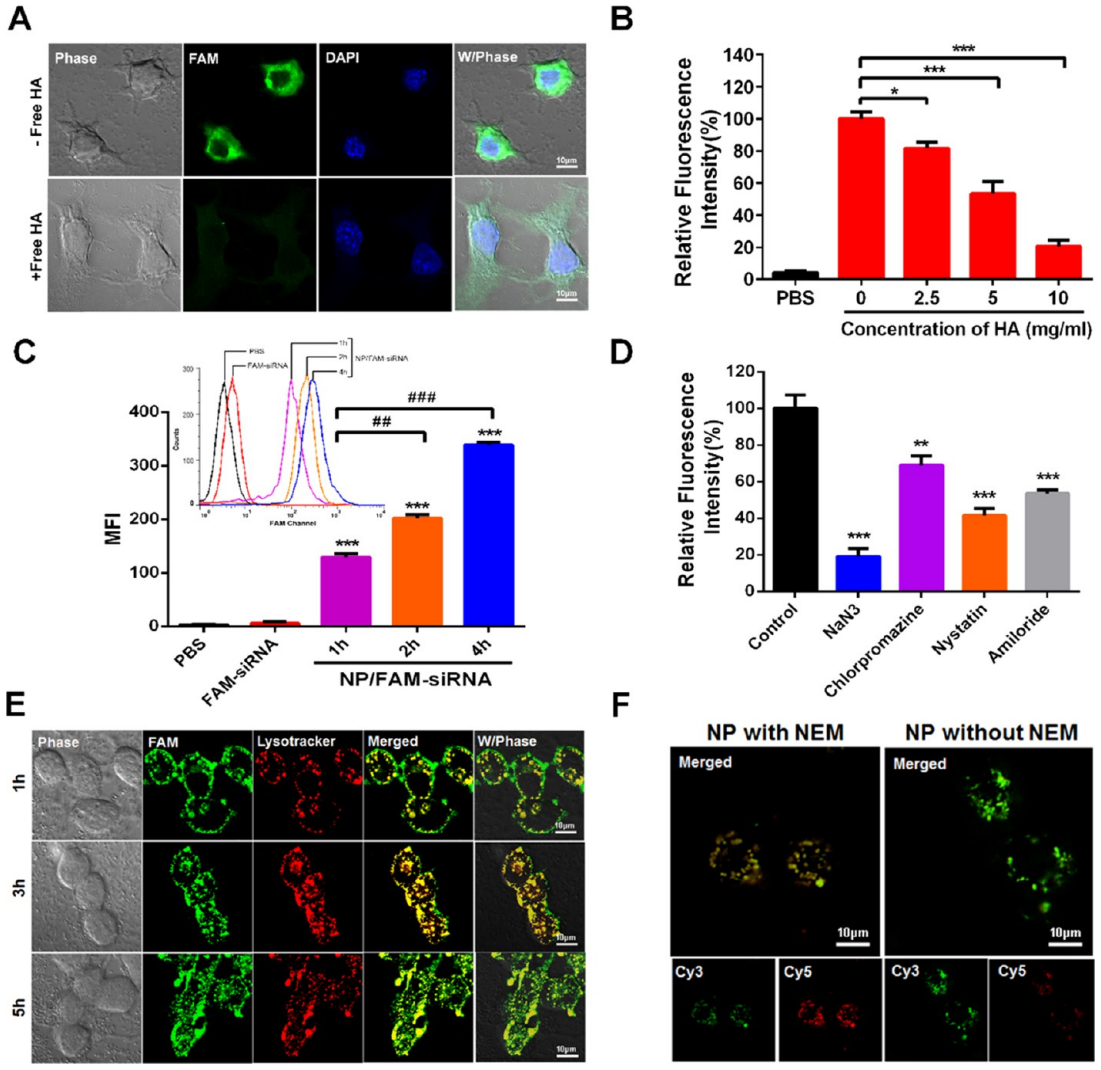

Figure 2. (A) Cell uptake of FAM-siRNA delivered by HA-SH/CaP nanoparticles with or without pretreatment by free HA. Images show the green fluorescence of FAM-siRNA and the blue fluorescence of DAPI in cell nuclei. The scale bar is 10 μm. (B) Effects of different concentrations of free HA on the uptake of $NP_{HA\text{-}SH/CaP}$/FAM-siRNA. Relative fluorescence intensity (%) = MFI (treated)/MFI (control) × 100% (n = 3). *p < 0.05, ***p < 0.005. (C) Cell uptake of $NP_{HA\text{-}SH/CaP}$/FAM-siRNA (siRNA = 100 nM) for different periods of time analyzed by flow cytometry. Data are shown as mean ± SD (n = 3). ***p < 0.005 vs FAM-siRNA group, $^{\#\#}p$ < 0.01, $^{\#\#\#}p$ < 0.005 vs 1 h incubation group. (D) Analysis of the endocytosis pathway of $NP_{HA\text{-}SH/CaP}$/FAM-siRNA determined by flow cytometry of cells treated with different endocytosis inhibitors. **p < 0.01, ***p < 0.005, compared with control group. (E) Endosomal escape of $NP_{HA\text{-}SH/CaP}$/FAM-siRNA (siRNA = 100 nM) in B16F10 cells. The late endosomes and lysosomes were stained with LysoTracker Red. Scale bar: 10 μm. (F) FRET analysis of the redox response of $NP_{HA\text{-}SH/CaP}$/siRNA. B16F10 cells were pretreated with or without the GSH inhibitor NEM, then incubated with NPs co-loaded with cy3- and cy5-labeled siRNA for 5 h, and visualized by CLSM. In the merged image, the yellow signal indicates co-localization of cy3-siRNA (green) and cy5-siRNA (red). Scale bar: 10 μm.

were mixed with siRNA and HA-SH. Hybrid nanoparticle solutions were purified by ultrafiltration for removing the free components.

The diameter of freshly prepared nanoparticles is about 216.3 ± 5.9 nm, and the PDI is 0.217. However, 12 h after preparation, the size decreased to 168.9 ± 1.2 nm and the PDI to 0.108 (Figure 1A). TEM was used to visualize directly the size and morphology of the siRNA-loaded nanoparticles. The spherical morphology of the nanoparticles is confirmed in Figure 1A. The observed size of the nanoparticles was approximately 150 nm, which was smaller than the hydrodynamic diameter obtained from the DLS. The bigger size of DLS than that of TEM may ascribe to the hydrated layer of HA-SS-HA. Particles of this size met the condition of the ERP effect that would mediate the accumulation of nanoparticles in tumor,[33] and HA can also actively target tumor cells that overexpress the CD44 receptor. The combination of passive and active targeting may allow our nanoparticles to accumulate at the tumor site, enabling selective delivery of drugs to cancer cells.[34] The surface ζ potential was −11.75 ± 0.82 mV (Figure 1B). This indicated the anionic nanoparticles had been successfully prepared, which is attributed to the excess free anionic carboxylic groups of thiolated-HA.

Anionic vectors have the same charge as nucleic acids, which greatly limits their application in gene delivery. CaP can condense nucleic acids with high efficiency. However, the poor colloidal stability of CaP nanoparticles limits their application for in vivo gene delivery. Herein, CaP was used to condense siRNA into hybrid nanoparticles, and the anionic HA-SH was used to stabilize the CaP nanoparticles. The EE% of siRNA by CaP was about 93% when the hybrid nanoparticles were assembled. The particle size decreased from 216 to 168 nm 12

DOI: 10.1021/acsami.6b15347
ACS Appl. Mater. Interfaces 2017, 9, 14576−14589

h after preparation, as shown in Figure 1C. This may be due to the cross-linking tightening effect caused by the oxidation of thiols and self-cross-linking of disulfide bonds in the air. The colloid stability of the nanoparticles was studied by DLS, following storage at 4 °C. The result indicated that the diameter of nanoparticles could remain around 200 nm for at least 5 days. However, CaP/siRNA and HA/CaP/siRNA nanoparticles were not stable at storage environment. Particle sizes of these groups increased quickly after preparation, which demonstrated the advantage of the cross-linked nanoparticles.

In addition to the colloidal stability, serum stability of different formulations was also studied. As shown in Figure S3, naked siRNA was quickly degraded in the absence of serum. Besides, the cross-linked nanoparticles HA-SS-HA/CaP/siRNA exhibited a better stability compared with CaP/siRNA and HA/CaP/siRNA formulations.

The stability of the siRNA in the nanoparticles after incubation with RNase for 0−48 h was checked by agarose gel electrophoresis. As shown in Figure 1D, no bands were visible on the gel before the nanoparticles were treated with SDS. The bands of each SDS-treated sample were as bright as free siRNA at 3 μM, even after 48 h incubation with RNase. We conclude that the HA-SS-HA/CaP/siRNA nanoparticles can effectively protect siRNA from serum destruction or RNase degradation, which is an important prerequisite for in vivo delivery of siRNA.

As shown in Figure 1E, the size of the cross-linked nanoparticles detected by DLS increased greatly after treatment with 10 mM of GSH. TEM revealed that no spherical particles were visible after GSH treatment. This suggested that the disulfide bonds of HA-ss-HA were destroyed by GSH and the structure of the nanoparticles became less compact. To test whether GSH treatment triggered siRNA release, the nanoparticles were incubated at pHs 5.0 and 7.4 with different GSH concentrations. As shown in Figure 1F, most of the siRNA encapsulated in the nanoparticles was released into the medium after incubation with 10 mM GSH for 2 h at pH 5.0 (the typical pH in lysosomes or endosomes). However, when $NP_{HA\text{-}SH/CaP}$/siRNA was incubated with or without 10 μM GSH at pH 7.4 (the typical pH of physiological environments), no obvious siRNA bands were observed. A weak siRNA band was found when the nanoparticles were incubated at pH 5.0 without GSH. This indicates that a small amount of siRNA was released from the siRNA/CaP complex, probably because the CaP dissolved slightly in the acid environment. All of the above suggested that GSH-triggered disruption of the HA-ss-HA shell and dissolution of the CaP core in acid environments may lead to a burst release of siRNA from nanoparticles.

Cellular Uptake, HA Competition, and Uptake Mechanism. CLSM was used to observe the uptake of siRNA-loaded nanoparticles in B16F10 cells. siRNA was labeled with FAM (green), and the nuclei were stained with DAPI (blue). After incubation for 2 h, the green fluorescence of FAM-siRNA was observed within the cytoplasm. It was previously reported that HA-associated nanoparticles can be efficiently taken up by receptor-mediated endocytosis in the body.[35] The cellular uptake of $NP_{HA\text{-}SH/CaP}$/FAM-siRNA was further investigated by a ligand competition experiment in the B16F10 cell line, which was reported to overexpress the CD44 receptor.[36,37] When the B16F10 cells were pretreated with a high dose of free HA (10 mg/mL) to block CD44 receptors prior to treatment with FAM-siRNA-loaded NPs, intracellular fluorescence was on a dime (Figure 2A), suggesting the decrease of cellular uptake of $NP_{HA\text{-}SH/CaP}$/FAM-siRNA. This result agrees well with previous reports on enhanced cancer cell-specific uptake of nanoparticles that are decorated on the surface with HA derivatives.[35,38,39] Flow cytometry was utilized to assess the inhibitory effect of pretreatment with different concentrations of HA upon nanoparticle uptake. As indicated in Figure 2B, the uptake of siRNA-NP decreased as the concentration of free HA increased in the range of 0−10 mg/mL. This further validated the role of the CD44 receptor in internalization of nanoparticles in B16F10 cells. Meanwhile, the mean fluorescence intensity (MFI) of $NP_{HA\text{-}SH/CaP}$/FAM-siRNA increased with longer incubation times (Figure 2C), indicating that the uptake of nanoparticles into B16F10 cell lines is time-dependent.

More importantly, understanding the endocytosis pathways is necessary to clarify the intracellular trafficking of $NP_{HA\text{-}SH/CaP}$/siRNA. As shown in Figure 2D, the internalization mechanism in B16F10 cells was evaluated using various inhibitors of specific cellular internalization pathways. After incubation with cell energy metabolism inhibitor (sodium azide), the uptake amount decreased sharply to 20% of that of the control, which indicated the energy-dependent endocytosis. The cellular uptake of $NP_{HA\text{-}SH/CaP}$/siRNA decreased to 45% of that of the control in the presence of nystatin, which is an inhibitor of caveolin-mediated endocytosis, indicating that the HA coating prompted the uptake of nanoparticles by the route of caveolin-mediated endocytosis. This result also demonstrated that HA was vital in the uptake of the nanoparticles. Chlorpromazine (clathrin-mediated endocytosis inhibitor) and amiloride (micropinocytosis inhibitor) also reduced the cellular uptake of nanoparticles. It can be concluded that $NP_{HA\text{-}SH/CaP}$ entered the cells through multiple pathways.

Endosomal Escape and Redox-Triggered Release. CLSM was further performed to determine whether HA-SH/CaP nanoparticles can effectively escape from endosomes or lysosomes. We evaluated the co-localization of the nanoparticles (green) in B16F10 cells with endosomes or lysosomes (red). As shown in Figure 2E, in the cells incubated with $NP_{HA\text{-}SH/CaP}$/FAM-siRNA for 3 h, the green fluorescence of FAM-siRNA encapsulated in HA-SH/CaP nanoparticles was mainly overlapped with the red signal of endosomes, indicating that $NP_{HA\text{-}SH/CaP}$/FAM-siRNA was effectively uptaken by the B16F10 cells and mainly distributed in endosomes. After incubation for another 2 h, the green signal (FAM-siRNA) was enhanced, whereas the yellow co-localization signal declined, demonstrating that FAM-siRNA had escaped successfully from the endosomes. The endosomal escape can be ascribed to disruption of the disulfide bonds in the HA-ss-HA shell and dissolution of the CaP core. The high concentration of the reducing agent in the tumor cells would disrupt the disulfide bonds in the shell so that the nanoparticles would become unstable. The CaP core would then be exposed to the acidic lysosomal or endosomal environment, resulting in disassembly of the nanoparticles. The calcium and phosphate ions would increase the osmotic pressure in the endosome, leading to its expansion and lysis so that siRNA is released into the cytoplasm.[14]

Inhibition of GSH-Dependent Reduction with NEM. FRET technology was used to validate the redox sensitivity of the nanoparticles. The fluorescence spectra (Figure S4) validated the FRET nanoparticles. In the cell study, siRNAs labeled with the donor dye cy3 (green) and acceptor dye cy5 (red) were co-encapsulated within the nanoparticles, which

DOI: 10.1021/acsami.6b15347
ACS Appl. Mater. Interfaces 2017, 9, 14576−14589

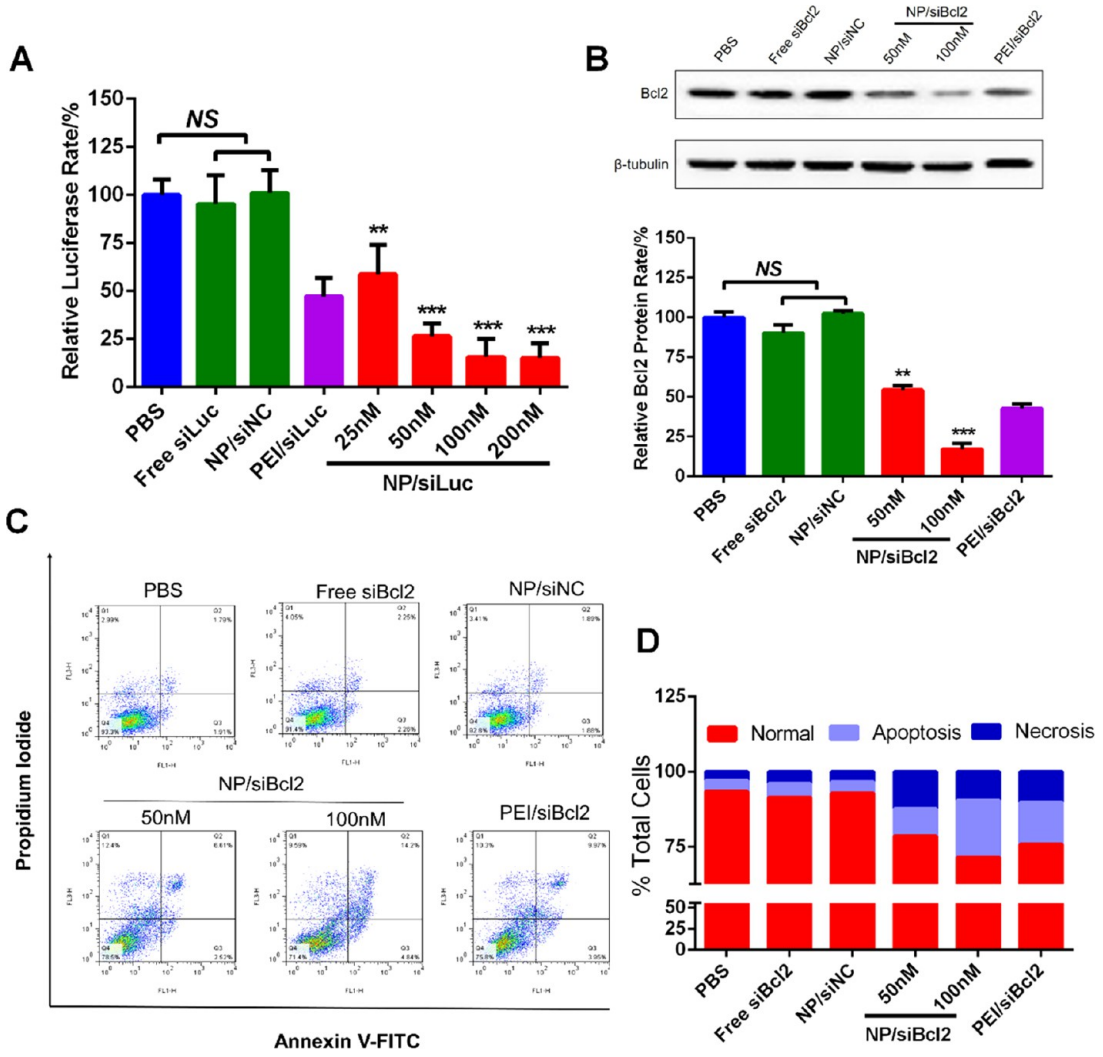

Figure 3. (A) Analysis of relative luciferase activity in B16F10-luciferase. siRNA concentrations of free siLuc and NP/siNC were 200 nM. PEI/siLuc indicates PEI 25 kDa (PEI/siRNA weight ratio = 1) mixed with siLuc (100 nM) as the positive control. $^{**}p < 0.01$, $^{***}p < 0.005$ vs NP/siNC group. (B) Western blot analysis of Bcl2 protein expression and semiquantitative analysis by Image J ($n = 3$). siRNA concentrations of PEI/siBcl2, free siBcl2, and NP/siNC were 100 nM. $^{**}p < 0.01$, $^{***}p < 0.005$ vs NP/siNC group. (C) Flow cytometry analysis of cell apoptosis after different treatments using the Annexin V-FITC/PI assay. siRNA concentrations of each group were the same as shown in (B). (D) Statistical analysis of normal, apoptotic, and necrotic cells. Data are shown as mean ± SD ($n = 3$).

were incubated for 2 h with B16F10 cells. FRET emission of the cy5 is observed only when the two dyes are co-encapsulated in the nanoparticles. As shown in Figure S5, we observed a relatively high intensity of red fluorescence (cy5-siRNA), indicating that the NPs were efficiently taken up by cells and that their integrity was maintained.

NEM, a GSH inhibitor, was used to deplete the GSH in the cells to establish the role of cytosolic reduction of $NP_{HA\text{-}SH/CaP}$/FAM-siRNA in the release of FAM-siRNA. As shown in Figure 2F, cells had a strong green fluorescence and weaker red fluorescence after 5 h of incubation without NEM pretreatment. This indicated that some of the nanoparticles had been disassembled so that the energy of cy3-siRNA could not be transferred to cy5-siRNA, leading to the observed weak fluorescence of cy5-siRNA (red). However, when the cells were pretreated with NEM, the red fluorescence of cy5-siRNA was much stronger, confirming the energy transfer from cy3-siRNA to cy5-siRNA in intact nanoparticles. This revealed that the stability of the nanoparticles within cells was maintained due to protection by the intact HA-ss-HA shell after depletion of GSH by NEM. The result is consistent with the in vitro siRNA release study in 3.2 (Figure 1F). Thus, the intracellular redox environment can effectively trigger the disassembly of HA-ss-HA nanoparticles and the release of siRNA.

Downregulation of Gene Expression and Induction of Cell Apoptosis in Vitro. The gene-silencing efficacy of $NP_{HA\text{-}SH/CaP}$/siRNA was evaluated using a luciferase kit and western blot analysis. B16F10-luciferase cells stably express luciferase. siLuc-loaded nanoparticles were incubated with B16F10-luciferase cells. As shown in Figure 3A, $NP_{HA\text{-}SH/CaP}$ carrying 100 nM of siLuc achieved a silencing efficacy of ~85%, which is even greater than our positive control, PEI 25 kDa. PEI 25 kDa carrying 100 nM of siLuc led to only ~53% knockdown of luciferase expression. The high silencing efficiency of $NP_{HA\text{-}SH/CaP}$ might be attributed to the enhanced uptake of the nanoparticles by CD44 receptors and effective escape of siRNA from lysosomes due to the redox-responsive property of HA-ss-HA and pH sensitivity of the CaP core. Furthermore, the silencing efficiency of $NP_{HA\text{-}SH/CaP}$/siLuc

DOI: 10.1021/acsami.6b15347
ACS Appl. Mater. Interfaces 2017, 9, 14576−14589

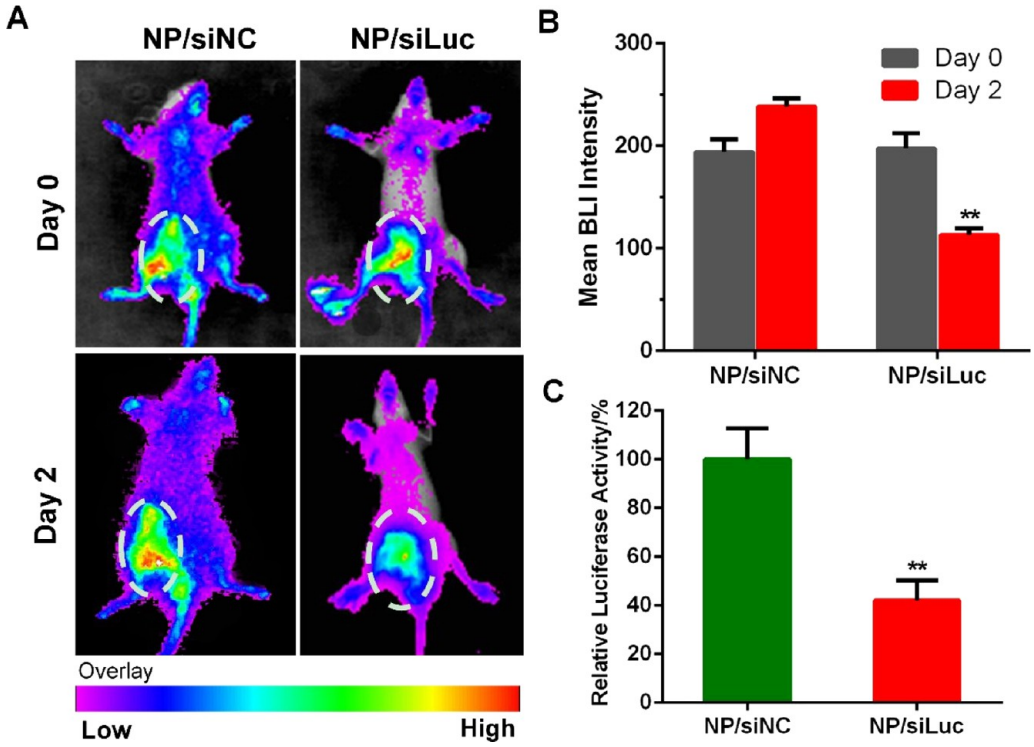

Figure 4. (A) Analysis of bioluminescence images of B16F10-luciferase xenograft tumors bearing mice. Images were obtained on days 0 and 2 (formulations were injected on days 0 and 1 separately). (B) Semiquantitative analysis of the image A. (C) On day 2 (24 h after the second injection), the tumors were removed from the mice and the luciferase activity in the tumor tissue was measured. Data are shown as mean ± SD (n = 3). $^{**}p < 0.01$, compared with NP/siNC on day 2.

increased with increasing siLuc concentration in the range of 25−200 nM.

To further investigate the therapeutic effect of the NPs, we choose the Bcl2 gene as our therapeutic target. Bcl2 protein has been widely certified as an antiapoptosis factor in malignant cells. The successful transfection of siRNA targeting Bcl2 can downregulate Bcl2 expression and induce cell apoptosis.[40] Here, B16F10 cells were incubated with $NP_{HA\text{-}SH/CaP}$/siBcl2, and the level of Bcl2 protein was analyzed by western blot after 48 h. As shown in Figure 3B, $NP_{HA\text{-}SH/CaP}$/siBcl2 significantly downregulated the expression of Bcl2 protein in B16F10 cells at both 50 and 100 nM and the effect was concentration-dependent. At a concentration of 100 nM, $NP_{HA\text{-}SH/CaP}$/siBcl2 reduced the Bcl2 protein level by ∼83%, whereas PEI 25 kDa reduced it by only ∼48%. The result of Bcl2 silencing was similar to that for the reporter gene luciferase.

Bcl2 is widely considered as a key factor in cancer cell survival; therefore, we measured the cell apoptosis induced by the downregulation of Bcl2 proteins by $NP_{HA\text{-}SH/CaP}$/siBcl2. B16F10 cells were double-stained with FITC-Annexin V and PI at 48 h after treatment with siBcl2-loaded nanoparticles. Cells that were positive only for FITC were considered to be in an early apoptotic phase and those positive only for PI were in necrosis phase. Consistent with Bcl2 silencing results, cells treated with $NP_{HA\text{-}SH/CaP}$/siBcl2 showed strong apoptosis and the level of cell apoptosis was dependent on the concentration of Bcl2 siRNA (Figure 3C,D). For cells treated with 100 nM of siBcl2 loaded in $NP_{HA\text{-}SH/CaP}$, a sum of the early and late apoptotic ratios was 19.01%. The percentage of apoptotic and necrotic cells in this group was about 30%, which showed that 100 nM of siBcl2 loaded into $NP_{HA\text{-}SH/CaP}$ can significantly increase the level of cell death. The effect of $NP_{HA\text{-}SH/CaP}$/siBcl2 (100 nM) was much stronger than that of the other treatments. These results confirm that $NP_{HA\text{-}SH/CaP}$/siBcl2 could induce cell apoptosis significantly.

In Vivo Luciferase Gene-Silencing Study. In vivo siRNA delivery and luciferase downregulation by $NP_{HA\text{-}SH/CaP}$/siLuc was studied in B16F10-luc tumor-bearing mice. As shown in Figure 4A,B, after two injections of $NP_{HA\text{-}SH/CaP}$/siLuc (siLuc 1.2 mg/kg), the intensity of bioluminescence decreased significantly. However, the $NP_{HA\text{-}SH/CaP}$/siNC group did not show decreased bioluminescence. On the contrary, the bioluminescence in the siNC-NP group became even stronger because of the growth of tumor. After the final image was taken, the tumors were extracted and the luciferase activity was detected with a Firefly Luciferase Assay Kit (Beyotime, Nanjing) (Figure 4C). The luciferase intensity in the $NP_{HA\text{-}SH/CaP}$/siLuc group was only 42% of that in the group treated with siNC-loaded nanoparticles, which meant that the level of luciferase enzyme expressed in the mice treated with siLuc NPs was 58% lower than that in the $NP_{HA\text{-}SH/CaP}$/siNC group. This was in accordance with the imaging result. Together, the results confirmed that the delivery of $NP_{HA\text{-}SH/CaP}$/siLuc to tumors caused the downregulation of luciferase.

In Vivo Antitumor Efficacy. From the in vivo luciferase gene-silencing experiment, we know that this delivery system can effectively carry siRNA to the tumor and achieve a specific silencing effect. To further investigate whether the system has potential for use in tumor therapy, we evaluated the antitumor efficacy of $NP_{HA\text{-}SH/CaP}$/siBcl2 in a B16F10 tumor xenograft model.[41,42] As shown in Figure 5A, tumor volumes increased rapidly in the $NP_{HA\text{-}SH/CaP}$/siNC and PBS groups, whereas $NP_{HA\text{-}SH/CaP}$/siBcl2 significantly inhibited tumor growth. More

DOI: 10.1021/acsami.6b15347
ACS Appl. Mater. Interfaces 2017, 9, 14576−14589

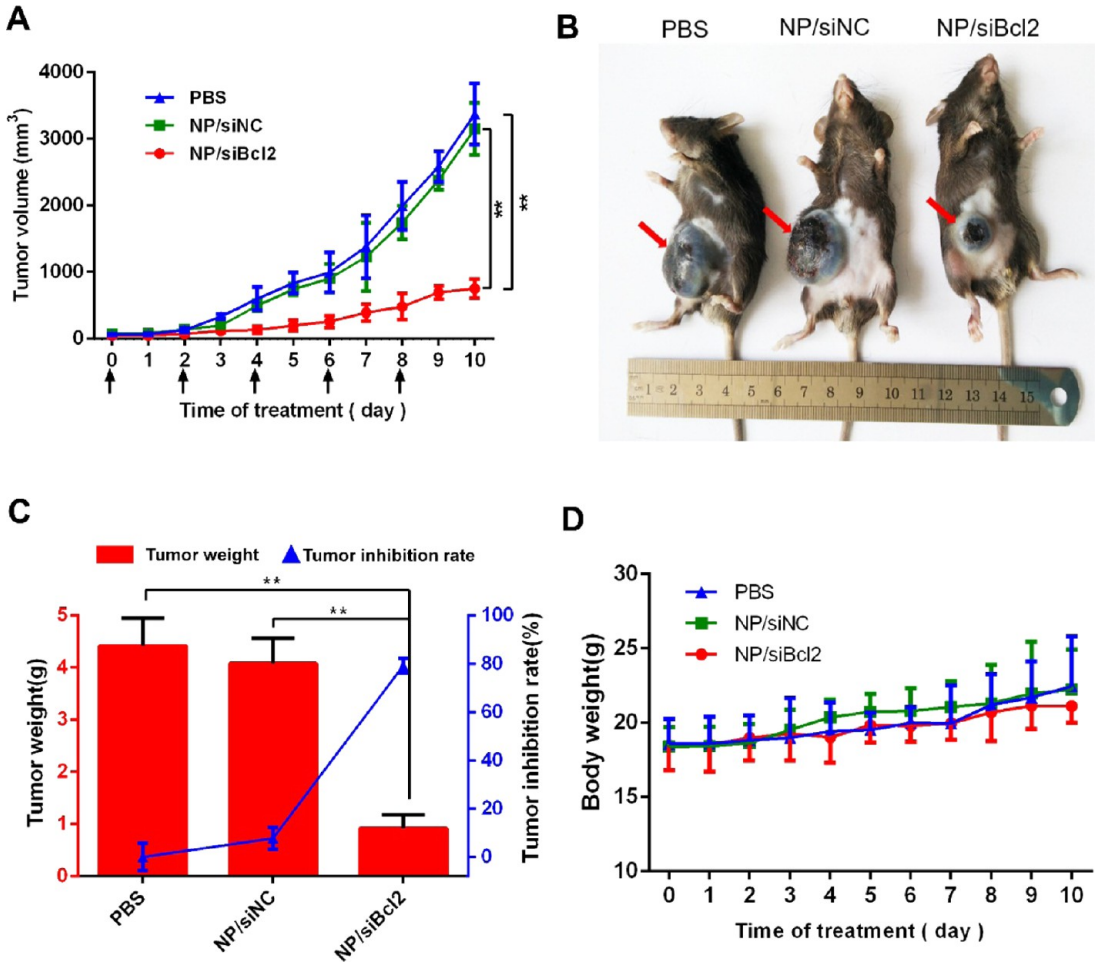

Figure 5. (A) B16F10 tumor growth curves of different groups after treatment on the indicated days (shown by arrows). siNC and siBcl2 were administered at a dose of 1.2 mg/kg. (B) Representative images taken on day 10 of the B16F10 xenograft tumors in mice treated with the different formulations. Arrows indicate the sites of tumors. (C) Tumor weight and the tumor inhibition rate analysis. (D) Graph showing the change in the body weights of B16F10 tumor-bearing mice over the treatment period. Data are shown as mean ± SD (n = 5). $^{**}p < 0.01$.

importantly, the photographs taken on day 10 show that the tumors in mice treated with $NP_{HA\text{-}SH/CaP}$/siBcl2 were noticeably smaller than those in the mice treated with PBS or $NP_{HA\text{-}SH/CaP}$/siNC (Figure 5B). This indicates that the delivery of siBcl2 by $NP_{HA\text{-}SH/CaP}$ was responsible for tumor growth suppression.

In the end, the tumors were separated from the body and weighed. The mass of tumors treated with $NP_{HA\text{-}SH/CaP}$/siBcl2 was only 25% of the tumor mass in the PBS or $NP_{HA\text{-}SH/CaP}$/siNC group and the tumor inhibition rate was about 80% (Figure 5C), which was calculated by the following formula: (the tumor weight of PBS group—the weight of treated group)/the weight of PBS group. There was no significant change in the body weight during treatment with $NP_{HA\text{-}SH/CaP}$/siBcl2 (Figure 5D), suggesting the low toxicity of the nanoparticles in vivo.

To validate that the tumor growth inhibition was owing to the Bcl2 gene silencing by $NP_{HA\text{-}SH/CaP}$/siBcl2, we used western blotting to check the expression of the Bcl2 protein in tumors treated with the different formulations. As shown in Figure 6A, there was a clear decrease in the Bcl2 protein level after treatment with $NP_{HA\text{-}SH/CaP}$/siBc2. The bands were also analyzed by Image J. The Bcl2 level was calculated as the intensity of Bcl2/intensity of β-tubulin, and the relative level was compared to that of the PBS group. The result showed that the Bcl2 protein was downregulated by about 60% by $NP_{HA\text{-}SH/CaP}$/siBcl2 (Figure 6B). $NP_{HA\text{-}SH/CaP}$/siNC did not cause any downregulation of Bcl2 protein expression compared to that caused by PBS.

We next analyzed H&E- and TUNEL-stained tumor sections (Figure 6C). The histological images indicated that after applying $NP_{HA\text{-}SH/CaP}$/siBcl2 a massive cancer cell remission occurred in the tumor tissue. Moreover, the images of TUNEL staining showed that the mice treated with $NP_{HA\text{-}SH/CaP}$/siBcl2 showed the highest level of cell apoptosis. This indicates that the superior tumor growth suppression was due to the significant apoptosis induced by $NP_{HA\text{-}SH/CaP}$/siBcl2.

Thus, we can conclude that the silencing of the antiapoptosis Bcl2 gene led to activation of apoptosis, which caused the noticeable tumor suppression effect.

Safety Evaluation. The $NP_{HA\text{-}SH/CaP}$ delivery system contains two components: (1) cationic Ca^{2+}, which autoassociates with siRNA to form the CaP core and (2) anionic HA-SH, which enhances the efficiency and stability of the CaP nanoparticles. Herein, the MTT assay was performed to assess the cytotoxicity of HA-SH and $NP_{HA\text{-}SH/CaP}$ to B16F10 cells. B16F10 cells were treated with different concentrations of HA-SH and no cytotoxicity was found even at the highest concentration, which was attributed to the good biocompatibility of HA-SH (Figure S6). In addition, after treatment of

DOI: 10.1021/acsami.6b15347
ACS Appl. Mater. Interfaces 2017, 9, 14576−14589

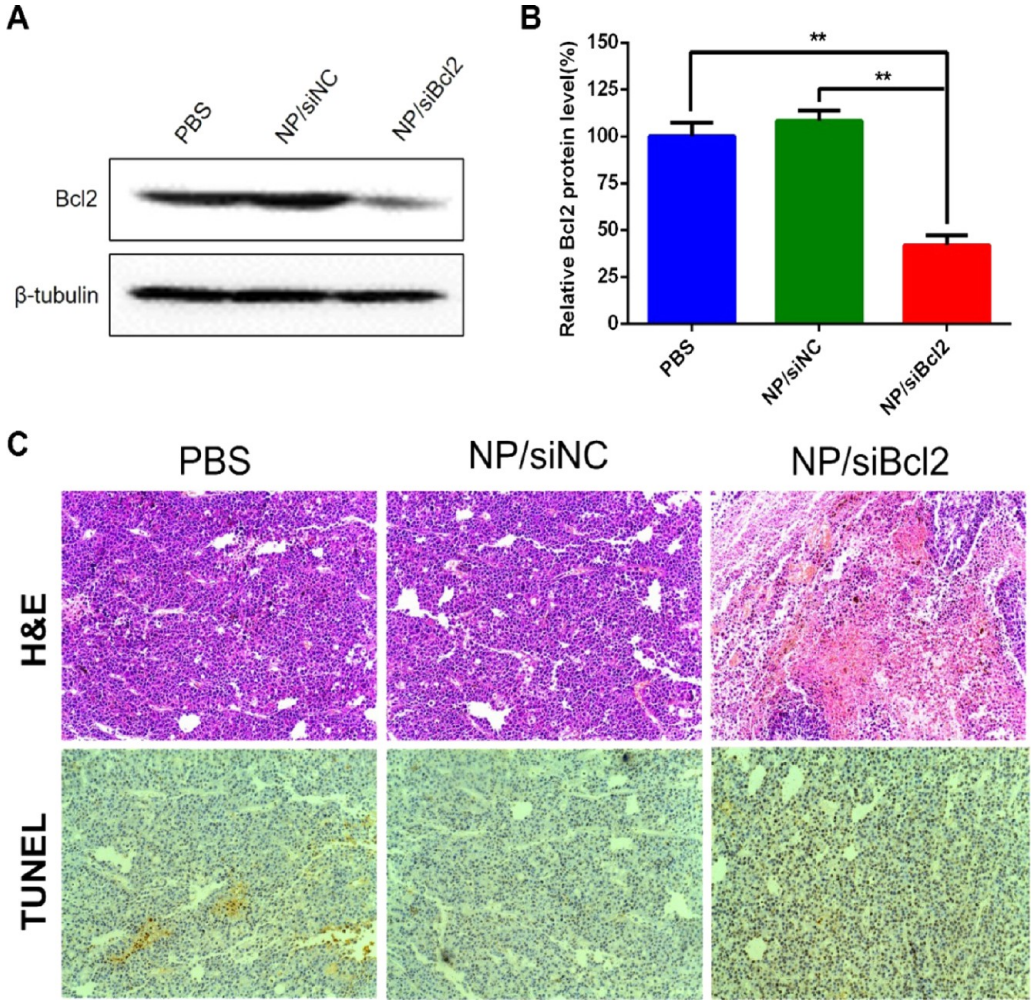

Figure 6. (A) Expression of Bcl2 protein in tumors after treatment with different formulations. (B) Semiquantitative analysis by Image J of (A). (C) Histological study of tumors after different treatment by the TUNEL assay and H&E staining. Data are shown as mean ± SD ($n = 5$). $^{**}p < 0.01$.

siNC nanoparticles, the viability of all of the groups was nearly 100%, which indicated the low cytotoxicity of $NP_{HA\text{-}SH/CaP}$ (Figure 7A). Although the disassembly of CaP nanoparticles in the tumor cells elevate the cytosolic Ca^{2+} concentration, researchers recently found that the calcium transporters pumped out the increased intracellular calcium, which prevented the toxicity.[43] In our previous work, we also proved that CaP/siNC nanoparticles stabilized by PEG-CMCS had no obvious toxicity to HepG2 cells.[14]

To test the in vivo applicability of our gene delivery system, we evaluated the toxicity of the HA-SH/CaP nanoparticles in healthy mice. Plasma levels of ALT, AST, and BUN were determined 24 h after three treatments with $NP_{HA\text{-}SH/CaP}$/siBcl2 via iv injection and compared with that of mice treated with PBS. As shown in Figure 7B, anionic nanoparticles produced results comparable to that of the PBS group, indicating that $NP_{HA\text{-}SH/CaP}$/siBcl2 did not have any obvious toxic effects on the liver or kidney at a therapeutic dosage. Furthermore, whole blood was collected from each mouse and routine blood tests were performed. As shown in Table 1, white blood cells (WBC), red blood cells (RBC), hemoglobin, platelets, neutrophils, and lymphocytes were analyzed. All of these blood indices in the $NP_{HA\text{-}SH/CaP}$/siBcl2 group were in the normal physiological range and were not significantly different from the values in the PBS group. We also harvested the main organs from the mice and examined the H&E-stained sections. Figure 7C shows that no significant difference was observed between these two groups. These results indicated that our nanoparticles did not cause organ toxicity. To sum up, our prepared cross-linked hybrid nanoparticles are safe for application both in vitro and in vivo.

CONCLUSIONS

In summary, we developed bioreducible cross-linked HA/CaP hybrid nanoparticles for active targeting delivery of siRNA in melanoma tumor therapy. The siRNA was efficaciously condensed by CaP, and the siRNA/CaP core was stabilized by the disulfide cross-linked HA-ss-HA shell. The nanoparticles were effectively delivered to cancer cells, and a burst of siRNA was released into the cytosol when breakage of the disulfide bonds was triggered by the high intracellular GSH concentration, followed by successful endosomal escape. We verified the hypothesis above by evaluating the combined effect of CD44-mediated cellular uptake and GSH-triggered controlled release in vitro and in vivo.

Anionic HA-ss-HA cross-linked nanoparticles were prepared by using CaP as a bridge to package siRNA into a positively charged core. The cross-linked hybrid nanoparticles could keep around 200 nm of volume for at least 5 days and showed superior protection effect on siRNA from RNase degradation.

DOI: 10.1021/acsami.6b15347
ACS Appl. Mater. Interfaces 2017, 9, 14576−14589

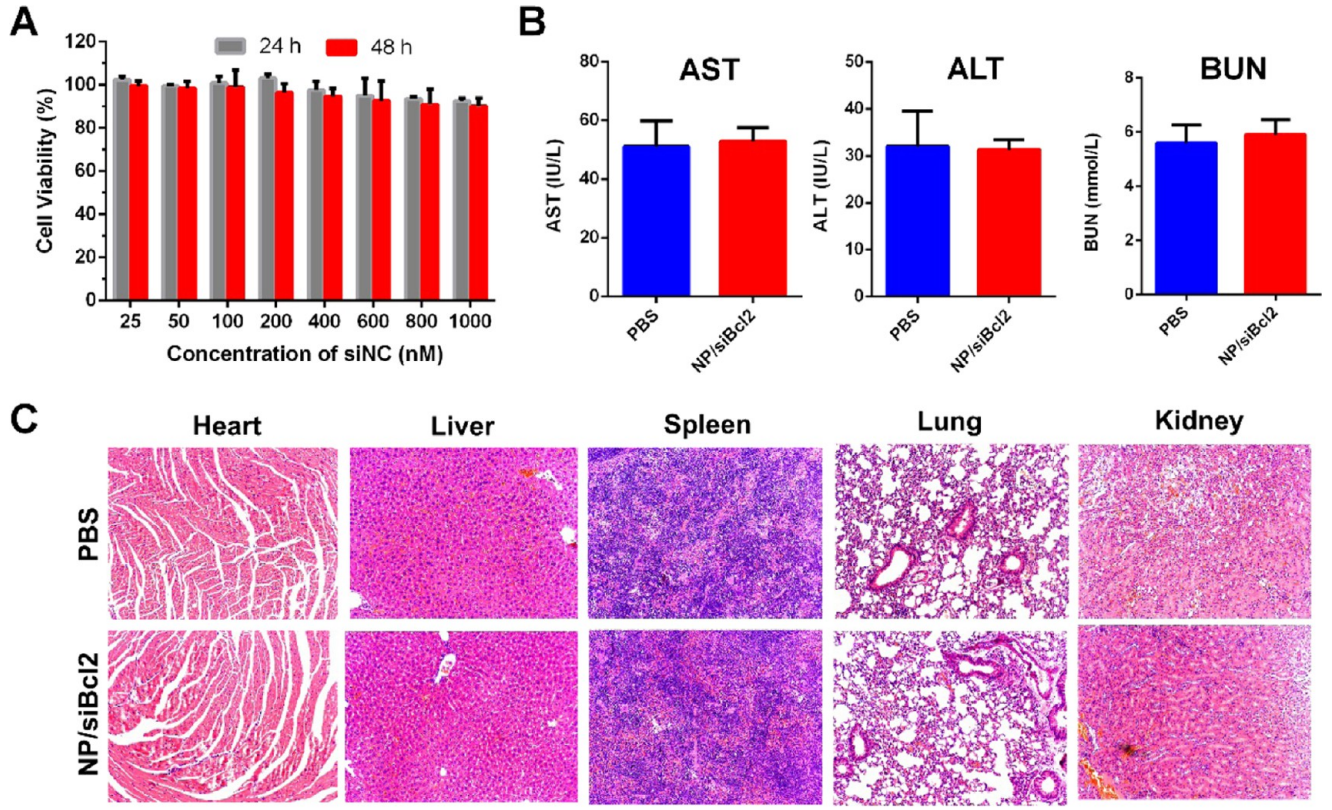

Figure 7. Safety evaluation. (A) In vitro cytotoxicity of $NP_{HA\text{-}SH/CaP}$/siNC to B16F10 cells. Data are shown as mean ± SD (n = 4). (B) Evaluation of liver functions (AST, ALT) and renal functions (BUN) in healthy mice after treatment with PBS or siBcl2-loaded nanoparticle. Data are shown as mean ± SD (n = 5). (C) Histological images of the HE-stained heart, liver, spleen, lung, and kidney harvested from the mice after treatment.

Table 1. Routine Blood Test Results of Mice after Treatment[a]

sample	WBC (10^9/L)	RBC (10^{12}/L)	hemoglobin (g/L)	platelet (10^9/L)	neutrophil (10^9/L)	lymphocyte (10^9/L)	monocyte (10^9/L)
PBS	5.18 ± 0.47	6.97 ± 0.35	112 ± 3.78	746 ± 79.68	0.56 ± 0.02	3.25 ± 0.48	0.07 ± 0.03
NP/siBcl2	5.24 ± 0.58	7.32 ± 0.19	115 ± 2.94	758 ± 68.42	0.53 ± 0.04	3.81 ± 0.39	0.08 ± 0.02

[a]Data are shown as mean ± SD, n = 5.

The particle-size variation, nanoparticle disassembly, and the burst of siRNA release in a GSH-rich environment confirmed the bioreducible property of the HA-ss-HA shell by using TEM, CLSM cell imaging, and agarose gel electrophoresis. Furthermore, $NP_{HA\text{-}SH/CaP}$ achieved a high siLuc silencing efficacy of ~85% and Bcl2 expression inhibition of ~83% at the protein level. In a xenograft tumor model, the in vivo intensity of bioluminescence in $NP_{HA\text{-}SH/CaP}$/siLuc-treated mice decreased significantly, whereas bioluminescence in mice treated with siNC nanoparticles became even more stronger as the tumor grew. The level of luciferase intensity in the $NP_{HA\text{-}SH/CaP}$/siLuc group was 58% lower than that in the $NP_{HA\text{-}SH/CaP}$/siNC group. Tumor growth was significantly inhibited by treatment with $NP_{HA\text{-}SH/CaP}$/siBcl2. Compared to that in the PBS or $NP_{HA\text{-}SH/CaP}$/siNC group, the tumor mass in the $NP_{HA\text{-}SH/CaP}$/siBcl2 group was just 25% and the Bcl2 protein expression level was 40%. More importantly, the prepared cross-linked hybrid nanoparticles are safe for application both in vitro and in vivo.

Overall, we have shown that the cross-linked HA-ss-HA-equipped CaP hybrid nanoparticles are simple and compact hybrid nanocarriers that possess multiple functions, such as redox responsiveness, endosomal escape, and tumor targeting, for gene delivery in antitumor therapy. This system has promising potential as a platform for gene delivery in targeted tumor therapy.

■ ASSOCIATED CONTENT

Supporting Information

The Supporting Information is available free of charge on the ACS Publications website at DOI: 10.1021/acsami.6b15347.

Synthesis procedure and characterization of HA-SH; degree of cross-linking of HA-SS-HA detection; serum stability of different formulations; fluorescence spectra of FRET nanoparticles; MTT assay of HA-SH on B16F10 cells (PDF)

■ AUTHOR INFORMATION

Corresponding Author

*E-mail: msun@cpu.edu.cn. Phone/Fax: +86 25 83271098.

ORCID

Hulin Jiang: 0000-0002-1620-1777

David Oupicky: 0000-0003-4710-861X

Notes

The authors declare no competing financial interest.

DOI: 10.1021/acsami.6b15347
ACS Appl. Mater. Interfaces 2017, 9, 14576−14589

■ ACKNOWLEDGMENTS

This work was supported by the National Natural Science Foundation of China (Nos. 81373983 and 81573377) and the Natural Science Foundation (No. 20141352) of Jiangsu Province and Six Talent Peaks Project (No. SWYY-011) of Jiangsu Province, Project Program of State Key Laboratory of Natural Medicines, China Pharmaceutical University (Nos. SKLNMZZJQ201603, SKLNMKF201608) and the Fundamental Research Funds for the Central Universities (No. 2016PT067).

■ REFERENCES

(1) McCormick, F. Cancer Gene Therapy: Fringe or Cutting Edge? *Nat. Rev. Cancer* **2001**, *1*, 130−141.
(2) Kim, H. J.; Kim, A.; Miyata, K.; Kataoka, K. Recent Progress in Development of siRNA Delivery Vehicles for Cancer Therapy. *Adv. Drug Delivery Rev.* **2016**, *104*, 61−77.
(3) Duerner, L. J.; Schwantes, A.; Schneider, I. C.; Cichutek, K.; Buchholz, C. J. Cell Entry Targeting Restricts Biodistribution of Replication-Competent Retroviruses to Tumour Tissue. *Gene Ther.* **2008**, *15*, 1500−1510.
(4) Lee, M. Y.; Park, S. J.; Park, K.; Kim, K. S.; Lee, H.; Hahn, S. K. Target-Specific Gene Silencing of Layer-by-Layer Assembled Gold-Cysteamine/siRNA/PEI/HA Nanocomplex. *ACS Nano* **2011**, *5*, 6138−6147.
(5) Wang, L. H.; Wu, D. C.; Xu, H. X.; You, Y. Z. High DNA-Binding Affinity and Gene-Transfection Efficacy of Bioreducible Cationic Nanomicelles with A Fluorinated Core. *Angew. Chem., Int. Ed.* **2016**, *55*, 755−759.
(6) Li, Y.; Lee, R. J.; Yu, K.; Ye, B.; Qi, Y.; Sun, Y.; Li, Y.; Jing, X.; Teng, L. Delivery of siRNA Using Lipid Nanoparticles Modified with Cell Penetrating Peptide. *ACS Appl. Mater. Interfaces* **2016**, *8*, 26613−26621.
(7) Epple, M.; Ganesan, K.; Heumann, R.; Klesing, J.; Kovtun, A.; Neumann, S.; Sokolova, V. Application of Calcium Phosphate Nanoparticles in Biomedicine. *J. Mater. Chem.* **2010**, *20*, 18−23.
(8) Forti, E.; Kryukov, O.; Elovic, E.; Goldstein, M.; Korin, E.; Margolis, G.; Felder, S.; Ruvinov, E.; Cohen, S. A Bridge to Silencing: Co-Assembling Anionic Nanoparticles of siRNA and Hyaluronan Sulfate via Calcium Bridges. *J. Controlled Release* **2016**, *232*, 215−227.
(9) Xie, Y.; Chen, Y.; Sun, M.; Ping, Q. A Mini Review of Biodegradable Calcium Phosphate Nanoparticles for Gene Delivery. *Curr. Pharm. Biotechnol.* **2013**, *14*, 918−925.
(10) Xu, X.; Li, Z.; Zhao, X.; Keen, L.; Kong, X. Calcium Phosphate Nanoparticles-Based Systems for siRNA Delivery. *Regener. Biomater.* **2016**, *3*, 187−195.
(11) Lee, M. S.; Lee, J. E.; Byun, E.; Kim, N. W.; Lee, K.; Lee, H.; Sim, S. J.; Lee, D. S.; Jeong, J. H. Target-Specific Delivery of siRNA by Stabilized Calcium Phosphate Nanoparticles Using Dopa-Hyaluronic Acid Conjugate. *J. Controlled Release* **2014**, *192*, 122−130.
(12) Li, J.; Yang, Y.; Huang, L. Calcium Phosphate Nanoparticles with An Asymmetric Lipid Bilayer Coating for siRNA Delivery to the Tumor. *J. Controlled Release* **2012**, *158*, 108−114.
(13) Zhang, M.; Ishii, A.; Nishiyama, N.; Matsumoto, S.; Ishii, T.; Yamasaki, Y.; Kataoka, K. PEGylated Calcium Phosphate Nanocomposites as Smart Environment-Sensitive Carriers for siRNA Delivery. *Adv. Mater.* **2009**, *21*, 3520−3525.
(14) Xie, Y.; Qiao, H.; Su, Z.; Chen, M.; Ping, Q.; Sun, M. PEGylated Carboxymethyl Chitosan/Calcium Phosphate Hybrid Anionic Nanoparticles Mediated hTERT siRNA Delivery for Anticancer Therapy. *Biomaterials* **2014**, *35*, 7978−7991.
(15) Milgrom, L. R. Towards Recombinant Antibody-Fragment Targeted Photodynamic Therapy. *Sci. Prog.* **2008**, *91*, 241−263.
(16) Jiang, X.; Li, L.; Liu, J.; Hennink, W. E.; Zhuo, R. Facile Fabrication of Thermo-Responsive and Reduction-Sensitive Polymeric Micelles for Anticancer Drug Delivery. *Macromol. Biosci.* **2012**, *12*, 703−711.
(17) Wang, J.; Yang, G.; Guo, X.; Tang, Z.; Zhong, Z.; Zhou, S. Redox-Responsive Polyanhydride Micelles for Cancer Therapy. *Biomaterials* **2014**, *35*, 3080−3090.
(18) Mura, S.; Nicolas, J.; Couvreur, P. Stimuli-Responsive Nanocarriers for Drug Delivery. *Nat. Mater.* **2013**, *12*, 991−1003.
(19) Arunachalam, B.; Phan, U. T.; Geuze, H. J.; Cresswell, P. Enzymatic Reduction of Disulfide Bonds in Lysosomes: Characterization of A Gamma-Interferon-Inducible Lysosomal Thiol Reductase (GILT). *Proc. Natl. Acad. Sci. U.S.A.* **2000**, *97*, 745−750.
(20) Cheng, R.; Feng, F.; Meng, F.; Deng, C.; Feijen, J.; Zhong, Z. Glutathione-Responsive Nano-Vehicles as A Promising Platform for Targeted Intracellular Drug and Gene Delivery. *J. Controlled Release* **2011**, *152*, 2−12.
(21) Oupický, D.; Li, J. Bioreducible Polycations in Nucleic Acid Delivery: Past, Present, and Future Trends. *Macromol. Biosci.* **2014**, *14*, 908.
(22) Sun, H.; Guo, B.; Cheng, R.; Meng, F.; Liu, H.; Zhong, Z. Biodegradable Micelles with Sheddable Poly(ethylene glycol) Shells for Triggered Intracellular Release of Doxorubicin. *Biomaterials* **2009**, *30*, 6358−6366.
(23) Zhang, P.; Zhang, H.; He, W.; Zhao, D.; Song, A.; Luan, Y. Disulfide-Linked Amphiphilic Polymer-Docetaxel Conjugates Assembled Redox-Sensitive Micelles for Efficient Antitumor Drug Delivery. *Biomacromolecules* **2016**, *17*, 1621−1632.
(24) Kim, E. J.; Shim, G.; Kim, K.; Kwon, I. C.; Oh, Y. K.; Shim, C. K. Hyaluronic Acid Complexed to Biodegradable Poly L-arginine for Targeted Delivery of siRNAs. *J. Gene Med.* **2009**, *11*, 791−803.
(25) Au, K. M.; Satterlee, A.; Min, Y.; Tian, X.; Kim, Y. S.; Caster, J. M.; Zhang, L.; Zhang, T.; Huang, L.; Wang, A. Z. Folate-Targeted pH-Responsive Calcium Zoledronate Nanoscale Metal-Organic Frameworks: Turning A Bone Antiresorptive Agent into An Anticancer Therapeutic. *Biomaterials* **2016**, *82*, 178−193.
(26) Zhong, Y.; Goltsche, K.; Cheng, L.; Xie, F.; Meng, F.; Deng, C.; Zhong, Z.; Haag, R. Hyaluronic Acid-Shelled Acid-Activatable Paclitaxel Prodrug Micelles Effectively Target and Treat CD44-Overexpressing Human Breast Tumor Xenografts in Vivo. *Biomaterials* **2016**, *84*, 250−261.
(27) Han, J.; Wang, Q.; Zhang, Z.; Gong, T.; Sun, X. Cationic Bovine Serum Albumin Based Self-Assembled Nanoparticles as siRNA Delivery Vector for Treating Lung Metastatic Cancer. *Small* **2014**, *10*, 524−535.
(28) Lee, H.; Choi, S. H.; Park, T. G. Direct Visualization of Hyaluronic Acid Polymer Chain by Self-Assembled One-Dimensional Array of Gold Nanoparticles. *Macromolecules* **2006**, *39*, 23−25.
(29) Verheul, R. J.; van der Wal, S.; Hennink, W. E. Tailorable Thiolated Trimethyl Chitosans for Covalently Stabilized Nanoparticles. *Biomacromolecules* **2010**, *11*, 1965−1971.
(30) Choi, K. Y.; Chung, H.; Min, K. H.; Yoon, H. Y.; Kim, K.; Park, J. H.; Kwon, I. C.; Jeong, S. Y. Self-Assembled Hyaluronic Acid Nanoparticles for Active Tumor Targeting. *Biomaterials* **2010**, *31*, 106−114.
(31) Gupta, M. K.; Meyer, T. A.; Nelson, C. E.; Duvall, C. L. Poly(PS-b-DMA) Micelles For Reactive Oxygen Species Triggered Drug Release. *J. Controlled Release* **2012**, *162*, 591−598.
(32) Nelson, C. E.; Kintzing, J. R.; Hanna, A.; Shannon, J. M.; Gupta, M. K.; Duvall, C. L. Balancing Cationic and Hydrophobic Content of PEGylated siRNA Polyplexes Enhances Endosome Escape, Stability, Blood Circulation Time, and Bioactivity in Vivo. *ACS Nano* **2013**, *7*, 8870−8880.
(33) Maeda, H.; Wu, J.; Sawa, T.; Matsumura, Y.; Hori, K. Tumor Vascular Permeability and the EPR Effect in Macromolecular Therapeutics: A Review. *J. Controlled Release* **2000**, *65*, 271−284.
(34) Skandalis, S. S.; Gialeli, C.; Theocharis, A. D.; Karamanos, N. K. Advances and Advantages of Nanomedicine in the Pharmacological Targeting of Hyaluronan-CD44 Interactions and Signaling in Cancer. *Adv. Cancer Res.* **2014**, *123*, 277−317.
(35) Eliaz, R. E.; Nir, S.; Szoka, F. C., Jr. Interactions of Hyaluronan-Targeted Liposomes with Cultured Cells: Modeling of Binding and Endocytosis. *Methods Enzymol.* **2004**, *387*, 16−33.

DOI: 10.1021/acsami.6b15347
ACS Appl. Mater. Interfaces 2017, 9, 14576−14589

(36) Choi, K. M.; Jang, M.; Kim, J. H.; Ahn, H. J. Tumor-Specific Delivery of siRNA Using Supramolecular Assembly of Hyaluronic Acid Nanoparticles and 2b RNA-Binding Protein/siRNA Complexes. *Biomaterials* **2014**, *35*, 7121−7132.
(37) Heo, R.; Yoon, H. Y.; Ko, H.; Shin, J. M.; Jeon, J.; Chae, Y. S.; Kang, Y. M.; Kim, D.; Lee, D. S.; Park, J. H. Gold-Installed Biostable Nanocomplexes for Tumor-Targeted siRNA Delivery in Vivo. *Chem. Commun.* **2015**, *51*, 16656−16659.
(38) Jiang, G.; Park, K.; Kim, J.; Kim, K. S.; Oh, E. J.; Kang, H.; Han, S. E.; Oh, Y. K.; Park, T. G.; Kwang Hahn, S. Hyaluronic Acid-Polyethyleneimine Conjugate for Target Specific Intracellular Delivery of siRNA. *Biopolymers* **2008**, *89*, 635−642.
(39) Yoon, H. Y.; Kim, H. R.; Saravanakumar, G.; Heo, R.; Chae, S. Y.; Um, W.; Kim, K.; Kwon, I. C.; Lee, J. Y.; Lee, D. S. Bioreducible Hyaluronic Acid Conjugates as siRNA Carrier for Tumor Targeting. *J. Controlled Release* **2013**, *172*, 653−661.
(40) Beloor, J.; Choi, C. S.; Nam, H. Y.; Park, M.; Kim, S. H.; Jackson, A.; Lee, K. Y.; Kim, S. W.; Kumar, P.; Lee, S. K. Arginine-Engrafted Biodegradable Polymer for the Systemic Delivery of Therapeutic siRNA. *Biomaterials* **2012**, *33*, 1640−1650.
(41) Wang, D.; Wang, T.; Liu, J.; Yu, H.; Jiao, S.; Feng, B.; Zhou, F.; Fu, Y.; Yin, Q.; Zhang, P.; Zhang, Z.; Zhou, Z.; Li, Y. Acid-Activatable Versatile Micelleplexes for PD-L1 Blockade-Enhanced Cancer Photodynamic Immunotherapy. *Nano Lett.* **2016**, *16*, 5503−5513.
(42) Shamay, Y.; Golan, M.; Tyomkin, D.; David, A. Assessing the Therapeutic Efficacy of VEGFR-1-Targeted Polymer Drug Conjugates in Mouse Tumor Models. *J. Controlled Release* **2016**, *229*, 192−199.
(43) Tseng, Y. C.; Yang, A.; Huang, L. How Does the Cell Overcome LCP Nanoparticle-Induced Calcium Toxicity? *Mol. Pharmaceutics* **2013**, *10*, 4391−4395.

DOI: 10.1021/acsami.6b15347
ACS Appl. Mater. Interfaces 2017, 9, 14576−14589